Tracking rotational diffusion of colloidal clusters

Gary L. Hunter,[1,*] **Kazem V. Edmond,**[1] **Mark T. Elsesser,**[2] **and Eric R. Weeks**[1]

[1]*Department of Physics, Emory University, Atlanta, Georgia 30322, USA*
[2]*Center for Soft Matter Research, Department of Physics, New York University, New York, New York 10003, USA*

[*]*glhunter@gmail.com*

Abstract: We describe a novel method of tracking the rotational motion of clusters of colloidal particles. Our method utilizes rigid body transformations to determine the rotations of a cluster and extends conventional proven particle tracking techniques in a simple way, thus facilitating the study of rotational dynamics in systems containing or composed of colloidal clusters. We test our method by measuring dynamical properties of simulated Brownian clusters under conditions relevant to microscopy experiments. We then use the technique to track and describe the motions of a real colloidal cluster imaged with confocal microscopy.

References and links

1. A. Kose, M. Ozaki, K. Takano, Y. Kobayashi, and S. Hachisu, "Direct observation of ordered latex suspension by metallurgical microscope," J. Colloid Interface Sci. **44**, 330–338 (1973).
2. D. J. W. Aastuen, N. A. Clark, L. K. Cotter, and B. J. Ackerson, "Nucleation and growth of colloidal crystals," Phys. Rev. Lett. **57**, 1733–1736 (1986).
3. C. A. Murray and D. H. Van Winkle, "Experimental observation of two-stage melting in a classical two-dimensional screened coulomb system," Phys. Rev. Lett. **58**, 1200–1203 (1987).
4. E. B. Sirota, H. D. O. Yang, S. K. Sinha, P. M. Chaikin, J. D. Axe, and Y. Fujii, "Complete phase diagram of a charged colloidal system: a synchrotron x-ray scattering study," Phys. Rev. Lett. **62**, 1524–1527 (1989).
5. P. N. Pusey and W. van Megen, "Phase behaviour of concentrated suspensions of nearly hard colloidal spheres," Nature **320**, 340–342 (1986).
6. P. N. Pusey and W. van Megen, "Observation of a glass transition in suspensions of spherical colloidal particles," Phys. Rev. Lett. **59**, 2083–2086 (1987).
7. P. N. Pusey, W. C. K. Poon, S. M. Ilett, and P. Bartlett, "Phase behaviour and structure of colloidal suspensions," J. Phys. Condens. Matter **6**, A29–A36 (1994).
8. E. R. Weeks, J. C. Crocker, A. C. Levitt, A. Schofield, and D. A. Weitz, "Three-dimensional direct imaging of structural relaxation near the colloidal glass transition," Science **287**, 627–631 (2000).
9. J. R. Savage, D. W. Blair, A. J. Levine, R. A. Guyer, and A. D. Dinsmore, "Imaging the sublimation dynamics of colloidal crystallites," Science **314**, 795–798 (2006).
10. D. H. Van Winkle and C. A. Murray, "Layering transitions in colloidal crystals as observed by diffraction and direct-lattice imaging," Phys. Rev. A **34**, 562–573 (1986).
11. C. A. Murray, W. O. Sprenger, and R. A. Wenk, "Comparison of melting in three and two dimensions: microscopy of colloidal spheres," Phys. Rev. B **42**, 688–703 (1990).
12. D. G. Grier and C. A. Murray, "The microscopic dynamics of freezing in supercooled colloidal fluids," J. Chem. Phys. **100**, 9088–9095 (1994).
13. U. Gasser, E. R. Weeks, A. Schofield, P. N. Pusey, and D. A. Weitz, "Real-space imaging of nucleation and growth in colloidal crystallization," Science **292**, 258–262 (2001).

14. J. Hernández-Guzmán and E. R. Weeks, "The equilibrium intrinsic crystal-liquid interface of colloids," Proc. Natl. Acad. Sci. U.S.A. **106**, 15198–15202 (2009).
15. J. C. Crocker and D. G. Grier, "Methods of digital video microscopy for colloidal studies," J. Colloid Interface Sci. **179**, 298–310 (1996).
16. A. D. Dinsmore, E. R. Weeks, V. Prasad, A. C. Levitt, and D. A. Weitz, "Three-dimensional confocal microscopy of colloids," Appl. Opt. **40**, 4152–4159 (2001).
17. E. R. Dufresne, T. M. Squires, M. P. Brenner, and D. G. Grier, "Hydrodynamic coupling of two Brownian spheres to a planar surface," Phys. Rev. Lett. **85**, 3317–3320 (2000).
18. C. R. Nugent, K. V. Edmond, H. N. Patel, and E. R. Weeks, "Colloidal glass transition observed in confinement," Phys. Rev. Lett. **99**, 025702 (2007).
19. R. Besseling, E. R. Weeks, A. B. Schofield, and W. C. K. Poon, "Three-dimensional imaging of colloidal glasses under steady shear," Phys. Rev. Lett. **99**, 028301 (2007).
20. P. Schall, D. A. Weitz, and F. Spaepen, "Structural rearrangements that govern flow in colloidal glasses," Science **318**, 1895–1899 (2007).
21. D. Chen, D. Semwogerere, J. Sato, V. Breedveld, and E. R. Weeks, "Microscopic structural relaxation in a sheared supercooled colloidal liquid," Phys. Rev. E **81**, 011403 (2010).
22. S. Martin, M. Reichert, H. Stark, and T. Gisler, "Direct observation of hydrodynamic rotation-translation coupling between two colloidal spheres," Phys. Rev. Lett. **97**, 248301 (2006).
23. S. M. Anthony, L. Hong, M. Kim, and S. Granick, "Single-particle colloid tracking in four dimensions," Langmuir **22**, 9812–9815 (2006).
24. P. J. Yunker, K. Chen, Z. Zhang, W. G. Ellenbroek, A. J. Liu, and A. G. Yodh, "Rotational and translational phonon modes in glasses composed of ellipsoidal particles," Phys. Rev. E **83**, 011403 (2011).
25. L. Hong, S. M. Anthony, and S. Granick, "Rotation in suspension of a rod-shaped colloid," Langmuir **22**, 7128–7131 (2006).
26. Y. Han, A. M. Alsayed, M. Nobili, J. Zhang, T. C. Lubensky, and A. G. Yodh, "Brownian motion of an ellipsoid," Science **314**, 626–630 (2006).
27. D. Mukhija and M. J. Solomon, "Translational and rotational dynamics of colloidal rods by direct visualization with confocal microscopy," J. Colloid Interface Sci. **314**, 98–106 (2007).
28. V. N. Manoharan, M. T. Elsesser, and D. J. Pine, "Dense packing and symmetry in small clusters of microspheres," Science **301**, 483–487 (2003).
29. M. T. Elsesser, A. D. Hollingsworth, K. V. Edmond, and D. J. Pine, "Large core-shell poly(methyl methacrylate) colloidal clusters: synthesis, characterization, and tracking," Langmuir **27**, 917–927 (2011).
30. A. van Blaaderen, "Chemistry: colloidal molecules and beyond," Science **301**, 470–471 (2003).
31. A. van Blaaderen, "Materials science: colloids get complex," Nature **439**, 545–546 (2006).
32. S. C. Glotzer and M. J. Solomon, "Anisotropy of building blocks and their assembly into complex structures," Nature Mater. **6**, 557–562 (2007).
33. S. M. Anthony, M. Kim, and S. Granick, "Translation-rotation decoupling of colloidal clusters of various symmetries," J. Chem. Phys. **129**, 244701 (2008).
34. J. Challis, "A procedure for determining rigid body transformation parameters," J. Biomech. **28**, 733–737 (1995).
35. HYDRO++, http://leonardo.inf.um.es/macromol/programs/hydro++/hydro++.htm .
36. M. G. Mazza, N. Giovambattista, F. W. Starr, and H. E. Stanley, "Relation between rotational and translational dynamic heterogeneities in water," Phys. Rev. Lett. **96**, 057803 (2006).
37. M. G. Mazza, N. Giovambattista, H. E. Stanley, and F. W. Starr, "Connection of translational and rotational dynamical heterogeneities with the breakdown of the Stokes–Einstein and Stokes–Einstein–Debye relations in water," Phys. Rev. E **76**, 031203 (2007).
38. S. Kämmerer, W. Kob, and R. Schilling, "Dynamics of the rotational degrees of freedom in a supercooled liquid of diatomic molecules," Phys. Rev. E **56**, 5450–5461 (1997).
39. B. J. Berne, P. Pechukas, and G. D. Harp, "Molecular reorientation in liquids and gases," J. Chem. Phys. **49**, 3125–3129 (1968).
40. G. Williams, "Time-correlation functions and molecular motions," Chem. Soc. Rev. **7**, 89–131 (1978).
41. M. Hoffmann, C. S. Wagner, L. Harnau, and A. Wittemann, "3D Brownian diffusion of submicron-sized particle clusters," ACS Nano **3**, 3326–3334 (2009).
42. F. Perrin, "Étude mathématique du mouvement Brownien de rotation," Ann. Sci. Ec. Normale Super. **45**, 1–51 (1928).

1. Introduction

Suspensions of spherical colloidal particles have proven a valuable model system for understanding many complex phenomena. Perhaps most notably, the model has provided insight into dynamical processes within different phases of matter [1–8], as well as various mechanisms involved during phase transitions [9–14]. A combination of digital video microscopy and com-

puterized particle tracking algorithms [15, 16] has allowed for the direct visualization of such colloidal systems and measurement of static and dynamical properties under many experimental conditions [17–21]. Given the spherical symmetry of the particles, most previous studies have understandably focused only on understanding translational dynamics, though there have been a few studies on rotational dynamics in dilute systems of spheres [22, 23], and on the translational and rotational dynamics of anisotropic colloidal particles [24–27].

Within the past decade, researchers have developed a variety of techniques for synthesizing clusters of colloidal particles with a wide range of reproducible morphologies [28, 29], several of which are shown in Fig. 1. Colloidal clusters have the potential to extend the colloidal model past one of simple spherical particles and into a realm where the collective dynamics of particles with complex shapes, more representative of molecules, can be studied [30–32].
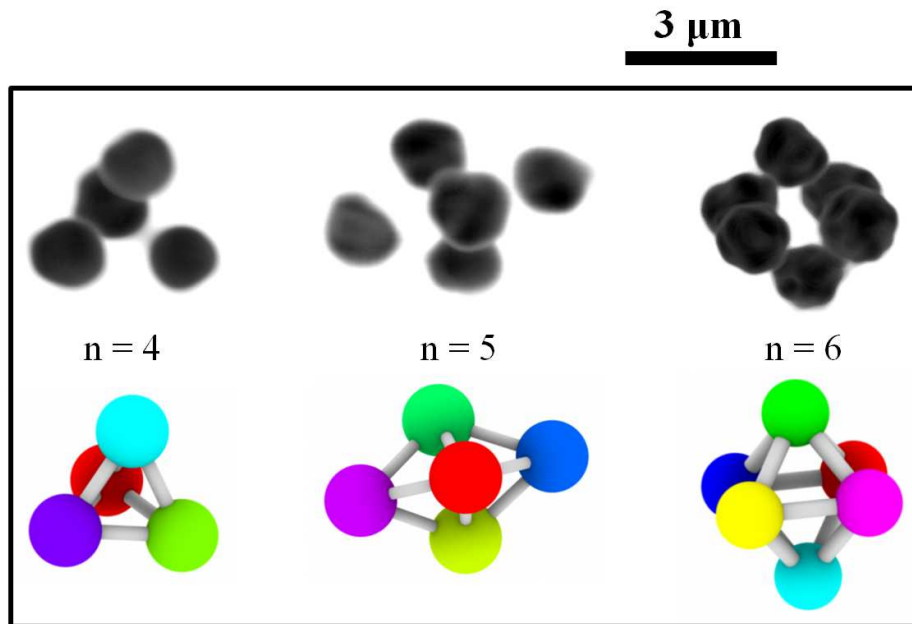

Fig. 1. Top: Volumetric images of colloidal clusters with $n = 4$, 5, and 6 from 3D confocal micrographs. Images have been filtered and enhanced to allow easy visualization of the 3-dimensional structures. Individual particles are approximately 2 μm in diameter. Bottom: Ball-and-stick models of the clusters above. The cases $n = 4$ and $n = 5$ are accurate representations of the simulated tetrahedra and pentahedra discussed in the text.

Conventional particle tracking methods [15, 16] are designed to follow the translational motions of individual particles, and so are immediately applicable to colloidal clusters, provided the particles can be reliably distinguished. However, a description of dynamics within systems composed of or including clusters is incomplete without knowledge of how rotational degrees of freedom are explored. Such an understanding could provide further insight into fundamental behaviors of systems with orientational order, such as liquid crystals, or systems subjected to external fields and anisotropic flows [27]. To our knowledge, there has been only one study that combined video microscopy with particle tracking to measure the rotational motion of colloidal clusters [33], using different methods than those described in this work. That study focused on dilute systems of planar clusters undergoing two-dimensional diffusion near a boundary, and revealed a decoupling of translational and rotational diffusion due to hydrodynamic effects.

We present here a simple and generalized method to track and calculate the two- or three-dimensional rotational motions of clusters of colloidal particles. Our method uses existing particle tracking routines and rigid body transformations to measure the changes in orientation of a cluster over time. To demonstrate the effectiveness and accuracy of the method, we simulate the motion of colloidal clusters under conditions that are relevant to microscopy experiments. We then use our method to measure the rotational diffusion coefficient of a real colloidal cluster.

2. Calculating rotations

Our procedure for calculating rotational displacements of clusters is based on a method by Challis for determining rigid body transformations between reference frames [34]. Challis' procedure was originally intended for comparing osteometric measurements in biomechanical analyses. As we will show, the method can be intuitively adapted to measure rotational dynamics. First, we give a brief reprise of Challis' method, and then describe how it is used to study the systems mentioned here.

2.1. Challis' procedure for coordinate transformations

Given a set of points which have coordinates $\{\mathbf{x}_i\}$ measured in one reference frame and coordinates $\{\mathbf{y}_i\}$ measured in a second frame, there exists a transformation

$$\mathbf{y}_i = s\mathbf{R}\mathbf{x}_i + \mathbf{v}, \tag{1}$$

where subscript i refers to the i-th point in the set, s is a scale factor, $\mathbf{R}$ is a 3×3 rotation matrix, and $\mathbf{v}$ is the vector separation of the two reference frames. For our purposes, we may set the scale factor to unity and assume that both coordinate frames share a common origin, thereby setting all elements of $\mathbf{v}$ to zero.

We are therefore left with

$$\mathbf{y}_i = \mathbf{R}\mathbf{x}_i, \tag{2}$$

and only the rotation matrix to describe the transformation between coordinate frames. The rotation matrix is an orthonormal matrix with the properties

$$\mathbf{R}\mathbf{R}^{-1} = \mathbf{R}\mathbf{R}^{\mathrm{T}} = \mathbf{R}^{\mathrm{T}}\mathbf{R} = \mathbf{E}, \tag{3}$$

$$\det(\mathbf{R}) = +1, \tag{4}$$

where $\mathbf{E}$ is the identity matrix and $\det()$ denotes the determinant.

For a set of n points, $\mathbf{R}$ can be calculated using a least squares approach. This method minimizes the quantity

$$\frac{1}{n}\sum_{i=1}^{n}[\mathbf{y}_i - \mathbf{R}\mathbf{x}_i]^{\mathrm{T}}[\mathbf{y}_i - \mathbf{R}\mathbf{x}_i]. \tag{5}$$

Ignoring the factor of $1/n$, expansion of Eq. (5) yields

$$\sum_{i=1}^{n}(\mathbf{y}_i)^{\mathrm{T}}\mathbf{y}_i + (\mathbf{x}_i)^{\mathrm{T}}\mathbf{x}_i - 2(\mathbf{y}_i)^{\mathrm{T}}\mathbf{R}\mathbf{x}_i. \tag{6}$$

Given that all $\mathbf{x}_i$ and $\mathbf{y}_i$ are fixed, minimizing Eq. (6) is therefore equivalent to maximizing

$$\sum_{i=1}^{n}(\mathbf{y}_i)^{\mathrm{T}}\mathbf{R}\mathbf{x}_i = \mathrm{Tr}\left(\mathbf{R}^{\mathrm{T}}\sum_{i=1}^{n}\mathbf{y}_i(\mathbf{x}_i)^{\mathrm{T}}\right) = \mathrm{Tr}(\mathbf{R}^{\mathrm{T}}\mathbf{C}), \tag{7}$$

where $\mathbf{C}$ is the cross-dispersion matrix calculated from the sum of the outer products of $\mathbf{y}_i$ and $\mathbf{x}_i^{\mathrm{T}}$

$$\mathbf{C} = \sum_{i=1}^{n} \mathbf{y}_i (\mathbf{x}_i)^{\mathrm{T}}. \tag{8}$$

At this point, a singular value decomposition (SVD) is performed on $\mathbf{C}$ such that

$$\mathbf{C} = \mathbf{U}\mathbf{W}\mathbf{V}^{\mathrm{T}}, \tag{9}$$

where $\mathbf{W}$ is a diagonal matrix containing the singular values of $\mathbf{C}$, and $\mathbf{U}$ and $\mathbf{V}$ are orthogonal matrices. As was shown in [34], upon maximizing Eq. (7), $\mathbf{R}$ is given by

$$\mathbf{R} = \mathbf{U} \begin{bmatrix} 1 & 0 & 0 \\ 0 & 1 & 0 \\ 0 & 0 & \det(\mathbf{U}\mathbf{V}^{\mathrm{T}}) \end{bmatrix} \mathbf{V}^{\mathrm{T}}. \tag{10}$$

This procedure is applicable to all non-colinear sets of points with $n \geq 3$.

2.2. Application to colloidal clusters

Particle tracking [15, 16] yields vector coordinates $\mathbf{x}_i'$ for every particle i over a distinct set of times. Hence, the first step in tracking rotational motion of a cluster is to track the translational motion of each particle within the cluster. For each cluster, we first determine the center of mass $\mathbf{x}_{CM}$ at a given time and subtract this quantity from the coordinates of particles belonging to the cluster, thereby removing any translational motion. We are left with new coordinates $\mathbf{x}_i$ in the center of mass frame,

$$\mathbf{x}_i = \mathbf{x}_i' - \mathbf{x}_{CM}. \tag{11}$$

This step is equivalent to setting the elements of $\mathbf{v}$ to zero in Eq. (1). With translational motion removed, we may apply Eq. (2) with a slightly different interpretation. Rather than representing a transformation between coordinate frames, we may understand $\mathbf{R}$ as describing the rotational trajectory of a particle with inital position $\mathbf{x}_i^0$ to a final position $\mathbf{x}_i$ such that

$$\mathbf{x}_i = \mathbf{R}\mathbf{x}_i^0. \tag{12}$$

Therefore, given the coordinates from a particle tracking experiment, we may use Challis' procedure, starting from Eq. (8), to calculate a cross dispersion matrix $\mathbf{C}$ and subsequently perform a singular value decomposition to calculate a rotation matrix for each pair of successive times $[t, t + \Delta t]$. With the complete set of rotation matrices, $\{\mathbf{R}^k\}$, we may reconstruct the entire trajectory of a particle about the cluster center of mass by computing the product of successive rotations. Given $\mathbf{x}_i^0$, the position of a particle at some later time t can be calculated as

$$\mathbf{x}_i(t) = \mathbf{R}^{t-\Delta t} \mathbf{R}^{t-2\Delta t} ... \mathbf{R}^0 \mathbf{x}_i^0 = \prod_k \mathbf{R}^k \mathbf{x}_i^0, \tag{13}$$

where the index k enumerates the rotation between successive times.

The advantage of calculating $\{\mathbf{R}^k\}$ is that it describes the collective behaviors of particles within a cluster, rather than a property of any individual particle. For example, knowledge of $\{\mathbf{R}^k\}$ for a cluster allows for immediate calculation of the motions of any particular particle about the center of mass, or the motion of the cluster about any arbitrary axis of rotation. Diffusive anisotropic clusters with large aspect ratios rotate more freely about a long axis than about a short axis. Given $\{\mathbf{R}^k\}$, however, one needs only the initial orientation of these axes to compute and compare the motions around them. An additional advantage of this procedure is that it is computationally fast, and the necessary linear algebra routines are standardly included in most mathematical software suites.

3. Tests of the prescribed method

For simplicity and to better reproduce the data collection process in typical microscopy experiments, we adopt a length scale of microns and a time scale measured in timesteps (ts), which is equivalent in microscopy to video frames or image stacks.

In conventional particle tracking experiments, it is important to minimize and understand the uncertainty, i.e. the noise, inherent in locating a particle. Typical microscopy experiments combine high magnification optics with CCD cameras to record raw digital images. In the absence of other sources of noise, the uncertainty in particle position, i.e. the minimum noise level, depends on the optical resolution [pixels/distance] of the instrumentation and the size [pixels] of the object being tracked. Standard image processing and particle tracking techniques can locate the centers of particles to within $\approx 1/N$ of a pixel, where N is the width of the object in pixels. Camera resolution varies between experimental set-ups but is typically in the range of 0.2 μm/pixel. The minimum uncertainty in particle position is the product of these factors. For example, observing a 10 pixel wide object with a resolution of 0.2 μm/pixel leads to a lower limit of ≈ 20 nm uncertainty in particle position. Other sources of noise, such as stray light entering the microscope, noise within the CCD camera itself, etc., slightly increase the uncertainty in particle position and further limit particle tracking resolution.

To test our method, we simulate the rotational Brownian motion of tetra- and pentahedral clusters with different rotational diffusion coefficients, D_R, and different levels of noise, σ_x. We first generate noise-free cluster trajectories. For tetrahedra, we place particles at initial coordinates

$$
\begin{aligned}
(R/\sqrt{3}) \cdot (1, \pm 1, \pm 1), \\
(R/\sqrt{3}) \cdot (-1, \pm 1, \mp 1),
\end{aligned}
\tag{14}
$$

where R is the distance from a particle center to the cluster center of mass. In this work, we study a range of $R \in [\sqrt{2}, \sqrt{10}]$ μm. For pentahedra, we use initial coordinates

$$
\begin{aligned}
R \cdot (1, 0, 0), \\
(R/2) \cdot (-1, \pm \sqrt{3}, 0), \\
R \cdot (0, 0, \pm 1).
\end{aligned}
\tag{15}
$$

Once initialized, we evolve each simulation for 10^4 time steps.

At each time step, we select three random angles, α, β, γ, from a Gaussian distribution with a standard deviation of $\sqrt{2D_R}$. This distribution ensures that the simulated dynamics will be in agreement with the Stokes-Einstein-Debye relation discussed later [Eq. (20)]. Each particle in a tetrahedron is rotated by an angle γ about the z-axis, then by an angle β about the y-axis, and finally by angle α about the x-axis to produce the tetrahedron at the subsequent time. The rotation matrices used are

$$
\mathbf{R}_x(\alpha) = \begin{pmatrix} 1 & 0 & 0 \\ 0 & \cos\alpha & -\sin\alpha \\ 0 & \sin\alpha & \cos\alpha \end{pmatrix}, \quad \mathbf{R}_y(\beta) = \begin{pmatrix} \cos\beta & 0 & \sin\beta \\ 0 & 1 & 0 \\ -\sin\beta & 0 & \cos\beta \end{pmatrix},
$$

$$
\mathbf{R}_z(\gamma) = \begin{pmatrix} \cos\gamma & -\sin\gamma & 0 \\ \sin\gamma & \cos\gamma & 0 \\ 0 & 0 & 1 \end{pmatrix}.
\tag{16}
$$

Thus, given an initial position vector $\mathbf{x}^0$, the subsequent position vector is $\mathbf{x} = \mathbf{R}_x \mathbf{R}_y \mathbf{R}_z \mathbf{x}^0$.

This method of generating rotational Brownian motion is not strictly correct for the given pentahedral geometry as its motions cannot be generally characterized by a single D_R. However, using the publicly available package HYDRO++ [35], we calculate the difference in D_R between long and short axes to be $\approx 2\%$. Given this small variation, the use of a single D_R to describe a pentahedron is a more than sufficient approximation for the purpose of testing our algorithm, which after all does not require that the motions agree with the laws of diffusion.

Trajectories generated in this way are noise-free in the sense that they are absent of uncertainty in particle position to within machine precision. To mimic the type of experimental noise previously mentioned, we post-process the trajectories by adding Gaussian random numbers, with standard deviation σ_x, to the particle coordinates. The levels of noise presented here correspond to uncertainties of $\sigma_x \in \{10,\ 30,\ 50,\ 70,\ 100\}$ nm in the x-, y-, and z-directions. Experimental uncertainties are typically within the range of 20-60 nm, and so the levels studied here are relevant to microscopy experiments. After the noise is added, we apply our method of measuring rotational motion in order to gauge the effect of experimental noise on results.

4. Analysis of rotational motion

In this section, we calculate the rotational motions of simulated colloidal clusters using the matrix methods described above. We focus on a method that uses the rotation matrices to determine the motion of a fictional orientation vector attached to the cluster. The rotational displacements of one or more such vectors about the center of mass can be used to compare and contrast motions about different axes, which is especially useful when the objects studied are anisotropic and motions about axes are expected to differ [36, 37].

We note that a second method exists to calculate rotational displacements using solely the rotation matrix. This method determines the rotational axis from $\mathbf{R}$ and can then be used to calculate the magnitude of an angular displacement. While a mathematically direct and general approach, it describes only the average cluster dynamics and can provide no insight into how motions about different axes vary. Given these limitations, we relegate a description of this method to the appendix.

To analyze the rotations of a cluster, we consider the motions of an initial orientational unit vector $\hat{\mathbf{p}}^0$ fixed to the cluster. We determine its orientation at a later time t by applying the set of rotations such that

$$\hat{\mathbf{p}}(t) = \prod_k \mathbf{R}^k \hat{\mathbf{p}}^0, \tag{17}$$

in a similar way as in Eq. (13). Although there are no constraints on what one may select $\hat{\mathbf{p}}^0$ to be, some choices may be more enlightening than others. For example, the cluster $n = 5$ shown in Fig. 1 has distinct long and short axes, and so one expects slower diffusion about the short axis. To quantify how rotational dynamics about these axes differ, one could choose two $\hat{\mathbf{p}}^0$ to study separately: one choice of $\hat{\mathbf{p}}^0$ perpendicular to the long axis; a second perpendicular to the short. Such a procedure would yield information relating to motions about the long and short axes, respectively.

In line with [36–38], we define a vector rotational displacement

$$\vec{\varphi}(t) = \int_0^t \vec{\omega}(t')dt' \tag{18}$$

in the time interval $[0,t]$. The vector $\vec{\omega}(t')dt'$ has a direction given by $\hat{\mathbf{p}}(t') \times \hat{\mathbf{p}}(t' + dt')$ and magnitude $|\vec{\omega}(t')dt'| = \cos^{-1}[\hat{\mathbf{p}}(t') \cdot \hat{\mathbf{p}}(t' + dt')]$, which is the angle subtended by $\hat{\mathbf{p}}$ during this time interval.

To illustrate the meaning of $\vec{\varphi}(t)$, consider an object with constant angular velocity $\vec{\omega} = \omega\hat{\mathbf{z}}$. Over a time Δt, the rotational vector displacement is given by $\vec{\varphi}(\Delta t) = \vec{\omega}\Delta t = (0,0,\omega\Delta t)$.
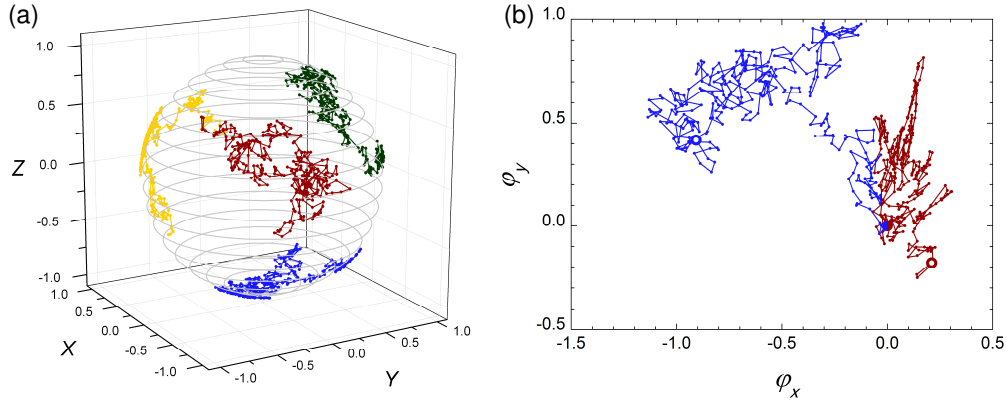
Fig. 2. (a) Trajectories of particles within a simulated Brownian tetrahedral cluster projected onto the surface of a unit sphere. Colors represent different particles, i.e. different choices for $\hat{\mathbf{p}}^0$. (b) 2d projection of two trajectories through rotation space (φ_x, φ_y). Colors correspond to the same particles in (a). Both trajectories in (b) begin at $(0,0)$ and end at open circles.

Therefore in general, $\vec{\varphi}(t)$ has components in each of the Cartesian axes, $(\varphi_x, \varphi_y, \varphi_z)$, corresponding to cumulative rotations about those axes.

In Fig. 2(a), we show the orientational trajectories of particles within a simulated tetrahedron projected onto the surface of a unit sphere. Fig. 2(b) shows 2D projections of trajectories for two $\hat{\mathbf{p}}^0$ through the rotation space described above. As shown in Fig. 2, even though the cluster is a solid body, trajectories of individual particles differ due to rotations of the cluster about random axes.

Given the definition of $\vec{\varphi}(t)$ in Eq. (18), we may define an unbounded mean square angular displacement (MSAD), akin to a translational mean square displacement, as

$$\langle \Delta\vec{\varphi}^2(\Delta t)\rangle = \langle [\vec{\varphi}(t+\Delta t) - \vec{\varphi}(t)]^2\rangle, \tag{19}$$

where the angle brackets indicate an average over all equivalent lag times Δt. In three dimensions the Stokes-Einstein-Debye relation states that the MSAD grows as

$$\langle \Delta\vec{\varphi}^2(\Delta t)\rangle = 4D_R\Delta t, \tag{20}$$

where D_R is the rotational diffusion coefficient. In this paper, we focus on measuring the MSADs of clusters, but we point out that other techniques exist to quantify rotational dynamics. For example, by observing the decay of an orientational correlation function $\langle \hat{\mathbf{p}}(t+\Delta t) \cdot \hat{\mathbf{p}}(t)\rangle$ one can measure D_R [39, 40]. Our method can be applied, in this case, to compute $\hat{\mathbf{p}}(t)$ as in Eq. (17).

In Fig. 3(a) & (b), we show the MSAD of two simulated tetrahedral clusters with diffusion constants 10^{-4} rad^2/ts and 10^{-3} rad^2/ts respectively and different levels of noise. The influence of noise is apparent in Fig. 3 as deviations from linearity at small Δt. Eventually, the MSAD recovers the true diffusive behavior because the cluster has made rotations large enough to distinguish from the noise.

With no experimental noise, a log-log plot of MSAD as a function of Δt will be a straight line with a slope of unity, as indicated by the open circles in Figs. 3(a) & (b). However, in the presence of noise in particle positions, rotations cannot be accurately resolved below a certain
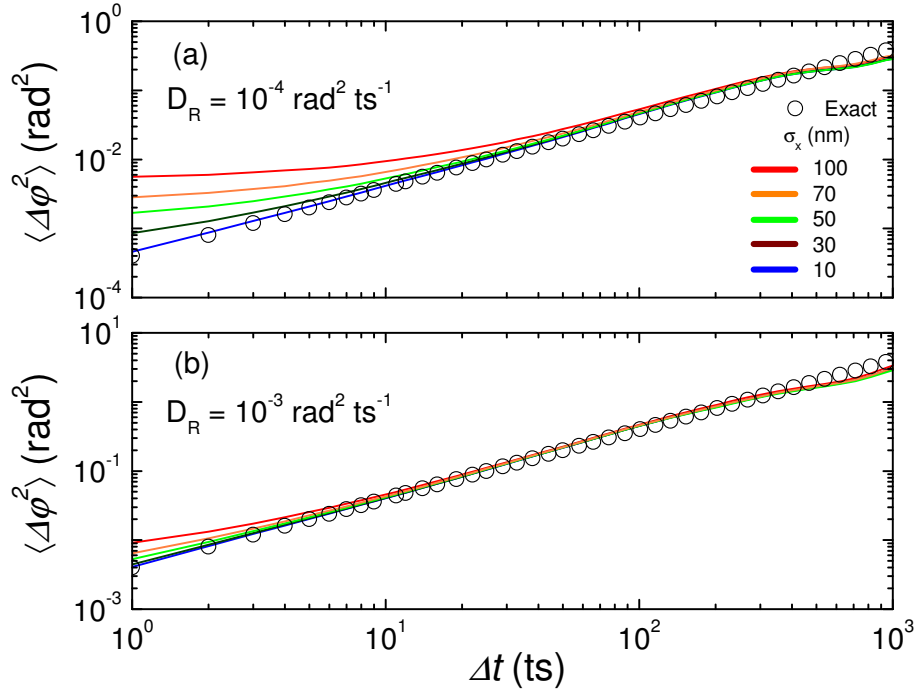
Fig. 3. Mean square angular displacements of simulated tetrahedral clusters ($R = \sqrt{3}\ \mu$m) for different noise levels σ_x and diffusion coefficients of (a) 10^{-4} rad^2/ts and (b) 10^{-3} rad^2/ts. Open circles are the theoretical MSAD based on Eq. (20). Deviations from linearity at small Δt demonstrate the effect of noise when resolving small rotations. Deviations at large Δt, however, are the result of low statistics at these lag times.

threshold, Φ. For example, a stationary cluster will appear to make small, but fictional, rotations as a result of this noise, and measurements of the MSAD will yield

$$\langle \Delta\vec{\varphi}^2(\Delta t)\rangle = \Phi^2, \tag{21}$$

where Φ^2 is independent of Δt due of the lack of correlations in noise.

In the case of translational diffusion, one expects that the noise in each direction will contribute an error of $2\sigma_x^2$ to the mean-square displacement [15]. In terms of an angular uncertainty, this contribution is diminished by a factor of R^2, where R is the average distance from a particle to the cluster center of mass. Our matrix method reduces this uncertainty further by a factor of n. Thus, when only static noise is present, one expects for a diffusing cluster

$$\langle \Delta\vec{\varphi}^2(\Delta t)\rangle = 4D_R\Delta t + \Phi^2, \tag{22}$$

where

$$\Phi^2 = 6\sigma_x^2/nR^2. \tag{23}$$

To test this assertion, we add noise to simulations of stationary ($D_R = 0$) tetrahedral clusters and calculate the MSADs. As in Eq. (21), the MSADs are constant over time. We take Φ^2 to be the value of the MSAD as $\Delta t \to 0$. Shown in Fig. 4(a), Eq. (23) accurately describes the static angular uncertainty for a wide range of tetra- and pentahedral cluster sizes, R, and noise
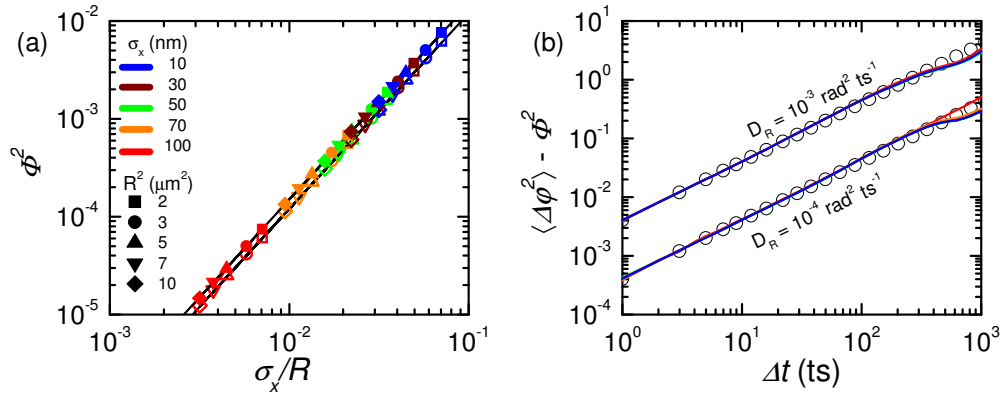
Fig. 4. (a) Measured values of Φ^2 for non-diffusing tetrahedral (solid symbols) and pentahedral (open symbols) clusters. Colors indicate noise levels and symbols indicate cluster size. Solid lines are the prediction $\Phi^2 = 6\sigma_x^2/nR^2$. (b) Same data in Fig. 3 with the appropriate Φ^2 for each noise level subtracted.

levels. Fig. 4(b) shows all of the previously measured MSADs in Fig. 3 plotted with the noise subtracted. This precisely collapses the MSADs to the true values in each case.

Knowing how uncertainty in particle positions affects measurements of dynamics quantities, such as the MSAD, is clearly important. However, one is typically unable to define the noise level so precisely in experiments. As stated earlier, particle tracking resolution depends on various experimental factors including particle size, optics, and the type of camera used to record images. As shown in Fig. 3(a), for slowly diffusing clusters and moderate-to-high noise levels, the measurements of the MSAD may not be representative of the true dynamics until fairly large lag times.

In microscopy experiments, one can effectively increase the rotational signal-to-noise ratio between each time step by imaging less frequently. Determining the appropriate sampling rates in experiments can be done by estimating the noise level σ_x, the diffusion constant D_R and calculating an approximate Φ^2. Diffusive motion will begin exceeding noise when $\Phi^2 \approx 4D_R\Delta t$. Solving for Δt then yields a reasonable sampling lag time. It is also important to avoid undersampling, that is, too long a lag time. Doing so will make diffusive motion between images appear erroneously slow. We find that a good rule of thumb for the upper limit on sampling time should be the time when the cluster has diffused ≈ 1 radian^2. Thus, an estimate for the upper limit is $\approx 1/4D_R$. However, as in all particle tracking experiments, the time between images must be small enough that individual particles can be confidently identified. This typically means that particles must be imaged before moving a distance of one interparticle spacing [15].

5. Experimental application

Measurements of rotational motion of diffusive tetrahedral clusters have been performed using the described method [29]. Real fluorescent tetrahedral clusters are synthesized as in [29]. A cluster is composed of individual poly(methyl methacrylate) (PMMA) spheres, each with a diameter 2.45 μm as measured by static light scattering (SLS). The particles within a cluster are irreversibly bound together, but are sterically stabilized to prevent the possibility of aggregation to other clusters. Dilute suspensions of clusters are prepared in a mixture of cyclohexyl bromide (CXB) and *cis*-decalin (DCL) at a ratio of 85/15 (w/w) that closely matches both the density and index of refraction of the particles. Clusters are imaged in 3D over time with a Leica TCS
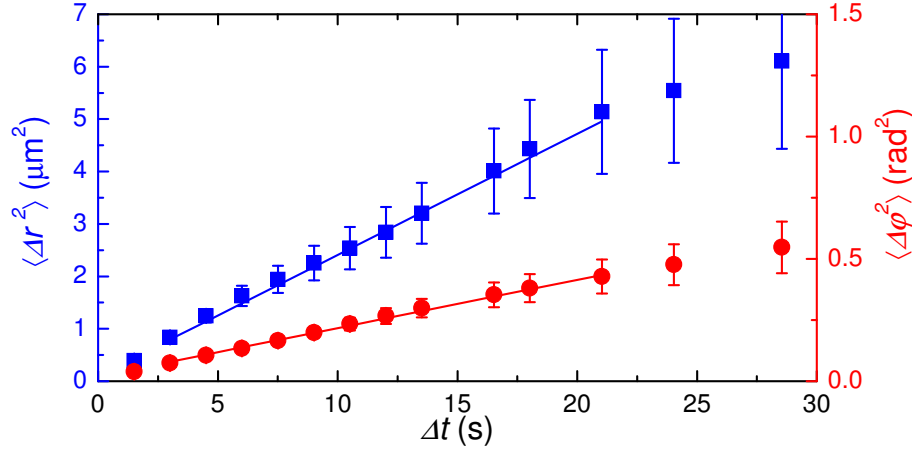
Fig. 5. Calculated MSD (blue squares) and MSAD (red circles) of a diffusing experimental tetrahedral cluster. Solid lines are best fit lines over range of data used to determine the respective diffusion coefficients.

SP5 confocal microscope. We track locations of the individual particles within a tetrahedron using standard particle tracking routines [15,16]. The uncertainties in particle position for these experiments are ≈ 30 nm in the x- and y-directions, and ≈ 40 nm in the z-direction. Given these tracking resolutions and assuming a maximally packed tetrahedron, from Eq. (23) we estimate the angular resolution in this experiment as $\Phi \approx 0.028$ radians ($1.6°$).

Once tracked, we calculate the translational MSD and the MSAD and determine the translational and rotational diffusion coefficients, D_T and D_R, respectively. In three dimensions, the translational MSD is described by the Stokes-Einstein-Sutherland equation

$$\langle \Delta r^2 \rangle = 6 D_T \Delta t, \tag{24}$$

while the MSAD is described by Eq. (20).

Hydrodynamically, tetrahedral clusters can be accurately modeled as spheres [41] given the relation

$$d_{\text{tetra}} = 1.844 \times d_{\text{sphere}}, \tag{25}$$

where d_{tetra} is the effective hydrodynamic diameter of the cluster, and d_{sphere} is the diameter of the particles within the cluster. Theoretical translational and rotational diffusion coefficients, D_T and D_R respectively, can be calculated using

$$D_T = \frac{k_B T}{3 \pi \eta d_{\text{tetra}}} \tag{26}$$

$$D_R = \frac{k_B T}{\pi \eta d_{\text{tetra}}^3}, \tag{27}$$

where k_B is Boltzmann's constant, T is the temperature, and η is the viscosity of the suspending solvent. The viscosity of the CXB/DCL mixture was measured at $\eta = 2.18$ mPas and experiments were performed at $T = 295$ K.

In Fig. 5, we show the MSD and MSAD of a diffusing tetradedral cluster. The MSD corresponds to motions of the center of mass of the cluster, and the MSAD is an average over the

individual particle MSADs (i.e., using the initial orientations of the particles as four separate $\hat{\mathbf{p}}^0$). Solid lines are fits to the data over the indicated range $3 \text{ s} \leq \Delta t \leq 22 \text{ s}$. As can be seen, both the MSD and MSAD are approximately linear only at small lag times. This is because the data set used to make these measurements consists of only a single cluster for less than 300 timesteps (≈ 220 s). Diffusion coefficients are measured by performing linear fits to the MSD and MSAD shown in Fig. 5 over the indicated range and extracting the slopes of the lines.

Table 1. Measurements from Tracking Tetrahedral Cluster

Diffusion	Coefficient	d_{tetra} (μm)	d_{sphere} (μm)
Trans.	$(3.85 \pm 0.49) \times 10^{-2}$ μm^2/s	5.12 ± 0.67	2.78 ± 0.36
Rot.	$(4.93 \pm 0.49) \times 10^{-3}$ rad^2/s	4.94 ± 0.16	2.68 ± 0.09

Shown in Table 1 are the measured translational and rotational diffusion coefficients. Values of d_{tetra} are calculated from Eqs. (26) & (27) using known experimental conditions, and values for d_{sphere} then follow trivially using Eq. (25). Ideally, the sizes calculated from translational motions would be identical to those calculated from rotational motions. As shown, these values agree to within 4%. Such good agreement between these two measurements demonstrates our ability to track translational and rotational motions of clusters simultaneously.

Previous work using standard particle tracking and our matrix method reported particle diameters $\approx 14\%$ larger than the 2.45 μm measured by SLS [29]. A reanalysis of the data with improved particle tracking, presented above, increases the accuracy of the particle diameter measured using our matrix method to within $\approx 9\%$. The remaining disagreement is likely due to multiple factors, including the fitting routines used in SLS and swelling of particles when in a solvent of CXB/DCL. SLS measurements were performed with suspensions in pure DCL, which is not known to swell particles.

6. Conclusion

We have presented a simple method of tracking the rotational motions of colloidal clusters. Our method implements conventional particle tracking routines to determine the locations of individual particles within a cluster and uses this information to compute rigid body transformations that describe changes in a cluster's orientation over time. The set of matrix transformations constitutes a global description of a cluster's motion during the course of an experiment or simulation and allows one to calculate rotational dynamics about any arbitrary axis. The least squares minimization used in this method considers the motions of each individual particle in calculating the rotation matrix, and therefore measurements of rotational displacements are less sensitive to tracking noise. Additionally, precision in determining angular displacements increases with cluster size R. When combined, the resolution of measuring angular displacements scales with $1/nR^2$.

Though constructed specifically for tracking colloidal clusters, we emphasize that our method is not limited to these systems, but is applicable to following the rotational motion of any body over time, providing that at least three distinct noncolinear points in the body can be reliably distinguished. Because the accuracy of tracking a rotation depends on the number of particles and the size of the body, the possibility exists that this method can be adapted to many-body systems where each particle diffuses independently of the rest while the system itself also undergoes bulk rotations. In this scenario, diffusive motions are random and can therefore be treated as noise while calculating $\{\mathbf{R}^k\}$ for the system. The rotation matrices can be inverted and, in a manner similar to Eq. (13), the bulk rotations can be removed, leaving only uncorrelated diffusive motion. Thus, this method is also applicable to determining particle motions in

rotating coordinate frames.

Appendix

Given a rotation matrix $\mathbf{R}$, one can calculate at each time the axis of rotation $\hat{\mathbf{u}}$ and angular displacement $\Delta\varphi$. In this notation, a rotational displacement can be described by a vector $\Delta\vec{\varphi} = \Delta\varphi\hat{\mathbf{u}}$, where $\hat{\mathbf{u}}$ has components in each of the Cartesian axes.

A single rotation will, by definition, have no effect on the direction of $\hat{\mathbf{u}}$, therefore,

$$\mathbf{R}\hat{\mathbf{u}} = \hat{\mathbf{u}}. \tag{28}$$

From Eq. (28), we see that the axis of rotation is an eigenvector of the matrix $\mathbf{R}$ with an eigenvalue of 1. For a set of rotational displacements $\{\mathbf{R}^k\}$, one may determine the axes of rotation by calculating the eigenvectors and eigenvalues of the rotation matrices, searching for the eigenvalues equal to 1, and taking the corresponding eigenvectors.

To determine the size of the displacement about the axis of rotation, one defines an arbitrary vector $\hat{\mathbf{w}}$ perpendicular to $\hat{\mathbf{u}}$. For simplicity, we choose $\hat{\mathbf{w}}$ to be perpendicular to the x-axis (denoted by $\hat{\mathbf{i}}$),

$$\hat{\mathbf{w}} = \frac{\hat{\mathbf{u}} \times \hat{\mathbf{i}}}{|\hat{\mathbf{u}} \times \hat{\mathbf{i}}|}. \tag{29}$$

and apply the rotation matrix,

$$\mathbf{R}\hat{\mathbf{w}} = \hat{\mathbf{w}}'. \tag{30}$$

The magnitude of the displacement is the angle between $\hat{\mathbf{w}}$ and $\hat{\mathbf{w}}'$, and can be computed using the cross product relation

$$\sin(\Delta\varphi)\hat{\mathbf{u}} = \hat{\mathbf{w}} \times \hat{\mathbf{w}}'. \tag{31}$$

Calculating displacements relative to the axis of rotation always results in displacements greater than or equal to those measured relative to an arbitrary $\hat{\mathbf{p}}^0$. For example, measuring a diffusion coefficient of a spherically symmetric body with this method will yield a value that is a factor of $3/2$ of the actual diffusion coefficient in Eq. (20).

To understand the origin of this difference, consider the rotational axis $\hat{\mathbf{u}} = \hat{\mathbf{z}}$, a perpendicular vector $\hat{\mathbf{w}} = \hat{\mathbf{x}}$, and an arbitrary vector $\hat{\mathbf{p}}^0$ located at Cartesian coordinates $(\sin\theta, 0, \cos\theta)$, where θ is the spherical polar angle. If $\hat{\mathbf{w}}$ is rotated by an amount $\delta\varphi_u$, the angle between $\hat{\mathbf{w}}$ and $\hat{\mathbf{w}}'$ is identically $\delta\varphi_u$. However, the angle $\delta\varphi$ between $\hat{\mathbf{p}}$ and $\hat{\mathbf{p}}'$ can be shown to be

$$\delta\varphi = \cos^{-1}\left(\sin^2\theta\cos\delta\varphi_u + \cos^2\theta\right) \tag{32}$$

For small $\delta\varphi_u$, we can approximate $\delta\varphi$ as

$$1 - \delta\varphi^2 \approx \sin^2\theta\left(1 - \delta\varphi_u^2\right) + \left(1 - \sin^2\theta\right) \tag{33}$$

$$\delta\varphi^2 \approx \sin^2\theta\,\delta\varphi_u^2. \tag{34}$$

If an average of Eq. (34) is taken over spherical coordinates, we are left with an expression similar to an MSAD,

$$\langle\delta\varphi^2\rangle = \langle\sin^2\theta\rangle\langle\delta\varphi_u^2\rangle = \frac{2}{3}\langle\delta\varphi_u^2\rangle, \tag{35}$$

The factor of $2/3$ arises for the same reasons in Perrin's original derivation of rotational diffusion [42]. Fig. 6 shows the MSADs measured in this way for two simulated pentahedral clusters, using a single diffusion constant for each. As stated, one can correct for the
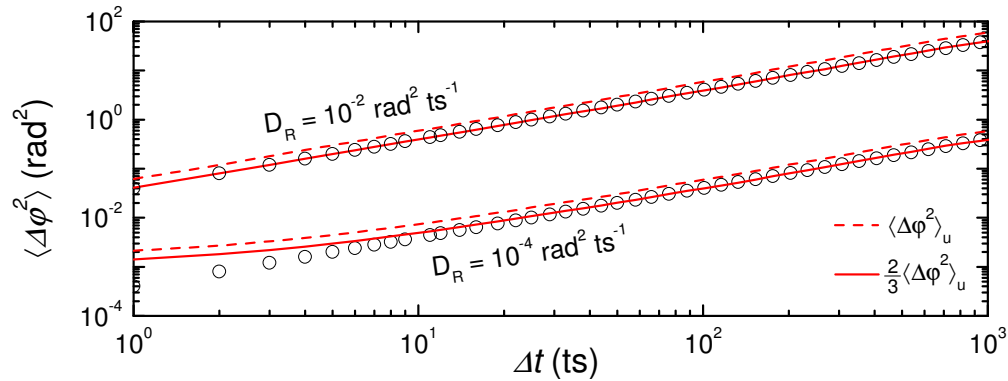
Fig. 6. The MSADs of simulated pentahedra ($R = \sqrt{3}\,\mu$m) with diffusion coefficients $D_R = 10^{-4}$ rad^2/ts and $D_R = 10^{-2}$ rad^2/ts and $\sigma_x = 50$ nm. Dashed lines show the uncorrected MSAD described below and solid lines are corrected data, obtained by multiplying the dashed lines by 2/3. Open circles are the theoretical MSAD from Eq. (20). We note that we have approximated diffusive motion by a single D_R for each pentahedron, as described in section 3.

overestimation of motion by simply multiplying the MSAD by 2/3. The average MSAD for any body can be corrected in the same manner, however we stress that this method returns only the average dynamics. While more direct than using an orientation vector, characterizing anisotropic bodies in this way will convolute motions about separate axes, and so will require some care when interpreting results.

Acknowledgements